Available online at www.sciencedirect.com
ScienceDirect
Magnetic Resonance Imaging 27 (2009) 994 – 1004
MAGNETIC RESONANCE IMAGING

A fully automated algorithm under modified FCM framework for improved brain MR image segmentation

Karan Sikka, Nitesh Sinha, Pankaj K. Singh, Amit K. Mishra*

Department of Electronics and Communication Engineering, Indian Institute of Technology Guwahati 781039, India

Received 3 November 2008; revised 6 January 2009; accepted 31 January 2009

Abstract

Automated brain magnetic resonance image (MRI) segmentation is a complex problem especially if accompanied by quality depreciating factors such as intensity inhomogeneity and noise. This article presents a new algorithm for automated segmentation of both normal and diseased brain MRI. An entropy driven homomorphic filtering technique has been employed in this work to remove the bias field. The initial cluster centers are estimated using a proposed algorithm called histogram-based local peak merger using adaptive window. Subsequently, a modified fuzzy *c*-mean (MFCM) technique using the neighborhood pixel considerations is applied. Finally, a new technique called neighborhood-based membership ambiguity correction (NMAC) has been used for smoothing the boundaries between different tissue classes as well as to remove small pixel level noise, which appear as misclassified pixels even after the MFCM approach. NMAC leads to much sharper boundaries between tissues and, hence, has been found to be highly effective in prominently estimating the tissue and tumor areas in a brain MR scan. The algorithm has been validated against MFCM and FMRIB software library using MRI scans from BrainWeb. Superior results to those achieved with MFCM technique have been observed along with the collateral advantages of fully automatic segmentation, faster computation and faster convergence of the objective function.
© 2009 Elsevier Inc. All rights reserved.

Keywords: FCM; MFCM; MRI; Segmentation; Homomorphic; Bias field

1. Introduction

The need to estimate morphological changes in brain tissues forms an important area of research. Various diseases are accompanied by size alterations in brain tissues. Examples of diseases belonging to this class include demyelinating diseases, transverse myelitis, schizophrenia, etc. [1,2]. Estimation of the expanse of brain tumors and lesions is also instrumental in the determination of dosage for treatment of such diseases. Estimation of tissue sizes thus forms an extremely important aspect of treatment which should be done as precisely as possible. This creates the need to properly segment the brain magnetic resonance image (MRI) into gray matter (GM), white matter (WM) and cerebrospinal fluid (CSF) and also to identify tumors or lesions, if present.

High contrast, high spatial resolution and multidimensionality have made MRI one of the most widely used techniques for clinical diagnosis. Manual estimation for detection of diminutive size changes in MR scans is prone to human error. The large amount of data also makes the task extremely cumbersome for human experts if done manually. In order to overcome this difficulty, various computer-analysis-based automatic and semiautomatic algorithms have been proposed over the years. The segmentation algorithms are broadly classified into two groups — supervised and unsupervised segmentation [3]. In the supervised approaches [4–8], a priori information is provided, which forms the basis of the segmentation process. Expectation maximization (EM) [8,7] and support vector machines [9] belong to this class of algorithms. The unsupervised approach [10,11] proceeds without any initial information, and segmentation is achieved with the

* Corresponding author.
E-mail addresses: k.sikka@iitg.ernet.in (K. Sikka), nitesh@iitg.ernet.in (N. Sinha), pankajk.s@iitg.ernet.in (P.K. Singh), amishra@iitg.ernet.in (A.K. Mishra).

0730-725X/$ – see front matter © 2009 Elsevier Inc. All rights reserved.
doi:10.1016/j.mri.2009.01.024

information extracted from the image itself. Examples of this class of approaches include k-mean clustering, fuzzy *c*-mean (FCM) clustering [12–14], etc.

Supervised techniques for segmentation suffer from the drawback of manual intervention for providing a priori information. These approaches assume a particular intensity distribution function of the pixels which may not always accurately fit the actual image intensity distribution. Unsupervised approaches are generally fast and do not require any a priori information. However, nonidealistic conditions lead to the presence of intensity inhomogeneities which culminates in intensity overlapping of different tissues. Further, noise also poses problem especially in conventional FCM approach where each pixel is dealt as a separate unit, independent of its spatial information. This leads to noisy segmented results.

In this article, we present an algorithm for fully automated brain MRI segmentation. For automatic estimation and subsequent removal of the bias field, the brain MR scan is passed through a entropy driven homomorphic filter [15]. This is followed by histogram truncation and redistribution based contrast enhancement (HTRCE). In this, the filtered image is iteratively tested for delivering a minimum value for a parameter called average variance. This value corresponds to optimized contrast enhancement in the bias corrected image. Once this is done, the number of tissue classes and their intensity centers in the filtered and contrasted image is estimated through its gray level histogram using a novel method named histogram based local peak merger (HLPM) which uses an adaptive window for automatically retrieving the cluster centers. The so obtained centers using the proposed method are fed as initial input to modified FCM (MFCM) clustering method [16]. This not only reduces the number of iterations but also shows a significant improvement in the segmentation results. Finally, another novel method for postprocessing named neighborhood based membership ambiguity correction (NMAC) is used which incorporates spatial information to smooth the boundaries between two tissue classes and also to remove pixel level noise present in the segmented results. The algorithm not only shows improved results on both simulated and real MRI but also has been found to correctly identify the number of tissue classes including tumors, lesions, etc. The strength of our algorithm lies in its simplicity along with ability to work with a wide array of brain MRIs.

Organization of the rest of the article is as follows. The following section gives an overview of the FCM algorithm followed by an overview of the MFCM algorithm in the next section. Section 4 explains our preprocessing and post-processing steps. It is complemented with the discussion of advantages of our proposed improvisations. In section 5, we validate the results from our algorithms against results from the well known FSL tool of Oxford University [17] and from MFCM. The test data consists of both simulated data from BrainWeb [18] and real MR scans. Discussions over the results on both T1- and T2-weighted images have been done.

2. Fuzzy *c*-mean clustering

FCM clustering technique imparts a degree of fuzziness to each data point corresponding to every cluster. The degree of fuzziness is represented by membership grade μ_{ij} such that

$$\sum_{j=1}^{c} \mu_{ij} = 1 \tag{1}$$

and,

$$\sum_{i=1}^{M} \mu_{ij} < M. \tag{2}$$

$\mu_{ij} \in (0,1)$ represents the membership grade of i'th pixel for j'th cluster. $i \in (1,\ldots,M)$, where M represents the total number of pixels in the gray-tone image. c is the number of cluster centers. Larger value of μ_{ij} implies greater proximity of the i'th pixel to the center of j'th cluster.

The aim of the algorithm is to find well-defined member grade for every pixel. This is done by iteratively minimizing an objective function given by

$$J_k = \sum_{i=1}^{M} \sum_{j=1}^{c} \mu_{ij}^{m} |x_i - w_j| \tag{3}$$

where, x_i is the gray scale intensity value of the i'th pixel and w_j is the cluster center of j'th cluster. m is called fuzzification parameter. It controls the noise sensitivity and the extent of the effect of μ_{ij} in the computation of cluster centers. k represents the iteration count. $m \in (1.5,2.5)$ has been found to be the optimal range for this parameter [19]. Correspondingly, $m = 2$ has been taken as it lies in the middle of the optimal range.

The minimization is done until the following condition is achieved:

$$|J_k - J_{k-1}| < \varepsilon |J_k - J_{(k-1)}| \tag{4}$$

The lower the value of ε, the greater is the degree of optimality achieved. $\varepsilon = 10^{-5}$ has been taken here.

To determine objective function, the matrix $U = [\mu_{ij}]$ and the vector $W = [w_j]$ are determined, which are given as

$$\mu_{ij} = \frac{\left(\frac{1}{(d_{ij})^2}\right)^{\frac{1}{(m-1)}}}{\sum_{j=1}^{c}\left(\frac{1}{(d_{ij})^2}\right)^{\frac{1}{(m-1)}}}, \tag{5}$$

$$w_{ij} = \frac{\sum_{i=1}^{M} \mu_{ij}^{m} x_i}{\sum_{j=1}^{M} \mu_{ij}^{m}} \tag{6}$$

where, d_{ij} is the distance between i'th pixel and j'th cluster center.

The matrix U and vector W corresponding to minimized objective function represents the final classification of pixels and cluster centers.

3. Modified FCM

Conventional FCM clustering technique suffers from the drawback of considering pixels as independent units. This makes it sensitive to noise. Previous works in literature find the solution to this problem using localized spatial information like neighborhood effect. In the methods proposed in [16,14], a pixel membership grade not only depends upon its own intensity but also on that of the neighboring pixels. The neighborhood consideration mitigates the effect of noise on a pixel. The membership grade of each pixel and the cluster center is updated using weight, p_{ij}, which represents the probability of i'th pixel belonging to j'th cluster and is determined using neighborhood model. The method proposed for determining weight p_{ij} is inspired from k-nearest neighbor (k-NN) algorithm and is computed according to the following formula

$$p_{ij} = \frac{\sum_{x_n \in N_i^j} \frac{1}{1+\alpha\left(d_{ij}\right)^2}}{\sum_{x_n \in N_i} \frac{1}{1+\alpha\left(d_{ij}\right)^2}}. \tag{7}$$

where, α is a positive constant, N_i is a set of k nearest pixels of the i'th pixel and, N_i^j *is the subset of* N_i *consisting of pixels belonging to j'th cluster.*

In each iteration, of conventional FCM, μ_{ij} is updated to μ_{ij}^* *according to following equation*

$$\mu_{ij}^* = \mu_{ij} p_{ij}. \tag{8}$$

The cluster center in the next iteration is updated accordingly using μ_{ij}^* in place of μ_{ij} according to Eq. (6).

4. Proposed algorithm

The MFCM approach dealt in the previous section has to be manually fed with the number of clusters. In this section, the innovative methods of contrast stretching (HTRCE), initial cluster center retrieval (using HLMP) and postprocessing (NMAC) have been discussed in detail.

4.1. Bias field estimation and contrast enhancement

In MR scans, spatial variations occur within the tissues of the same class due to inhomogeneity in the excitation field caused by physical imperfections in RF coils of the MRI machine. Many methods have been proposed and tested to remove this artifact [20]. The most archaic method for the removal of bias field is the measurement of the coil insensitivity using a physical phantom [21]. The primary drawbacks with this method is that manual feeding of this phantom is required for the subsequent algorithm. The method proposed by Wells et al. [7] and later modified by Guillemard and Brady [22] made the use of a priori model of the brain tissues (atlas) [8] and maximum likelihood criterion for estimation and correction of the bias field. The drawback of this method is that the a priori knowledge of tissue classes is required, which, if not given correctly, may cause the EM algorithm to converge early and erroneously. Though methods employing neighborhood consideration, for example, algorithms using Markov random fields (MRF) [23], show improved results, they are known to be computationally intensive. The FCM methods that incorporate the bias field considerations in their objective function may not be able to identify separate regions other than WM, GM and CSF, like tumors and lesions [14]. A common example is an attempt to model the bias field as a smooth function using Legendres polynomial [24], splines surfaces [25], etc. As more degrees of freedom are added, the method becomes computationally more demanding and local minima in the optimization become a cause of common error.

An extensive research done on different methods of bias field removal [20] found that none of the methods proved to be acceptably generic. The bias field has been found to be slowly varying and should be removed prior to segmentation as it leads to intensity overlapping among different tissue-classes. In this paper we have used exponential entropy driven Homomorphic Unsharp Masking (HUM) [15] as a pre-processing tool for eliminating the field followed by contrast stretching.

The bias field being a slowly varying field can be seen as a low-pass multiplicative noise. An image can be expressed as the product of illuminance and reflectance.

$$I(x,y) = i_0 \cdot i(x,y) \cdot r(x,y). \tag{9}$$

Here, I (x,y) is the observed image intensity at spatial location (x,y), i_0 is the desired constant illumination and r is reflectance of the image. The artifact introduced by coil inhomogeneity is given by $i(x,y)$ [26].

Since we intend to use filtering technique for the elimination of the bias field, the procedure cannot be implemented directly due to the multiplicative nature of bias field. For this, the image is manipulated in the logarithmic domain where the inhomogeneity becomes additive and is removed by a suitable filter.

$$\begin{gathered} G(x,y) = \log[I(x,y)] = \log(i_0) + \log[i(x,y)] + \log[r(x,y)], \\ G_{\text{bias}}(x,y) = \text{IDFT}\{\text{DFT}[G(x,y)][H(u,v)]\}, \\ I' = G - G_{\text{bias}}, \\ I_{\text{cor}} = exp(I'). \end{gathered} \tag{10}$$

Here, DFT is discrete Fourier transform and IDFT is inverse discrete Fourier transform. H (u,v) is the Butterworth realization of low-pass filter, I' is the log transform of the bias free image, I_{cor} is the bias corrected image and G_{bias} is a log transform of the bias field.

For finding the cutoff frequency of the filter, Butterworth filter cutoff frequency method based on local entropy measure [15] has been employed and was found to give good results.

The above process is followed by contrast stretching. Though a number of techniques exist for contrast enhancement [27], most of them do not perform satisfactorily with the problem in hand.

This problem was handled by an algorithm proposed in the current work named HTRCE. In this algorithm, contrast stretching is achieved by truncating the ends of the histogram of the image and renormalizing it. An optimal value for the degree of stretching required is estimated by iteratively minimizing a quantity called average variance, which we define as

$$avar = \sum_{j=1}^{c} \frac{\sum_{i=m_j}^{n_j} |H_i - \phi_j|^2}{\sum_{i=m_j}^{n_j} H_i} \tag{11}$$

where,

$$\phi = \frac{\sum_{i=m_j}^{n_j} H_i}{n_j - m_j}. \tag{12}$$

Here, the range of i from m_j to n_j represents the bin positions in the histogram of the image that lie in the j'th cluster according to the initial U matrix. H_i represents the value of the histogram at the i'th bin. Determination of c is done using automatic retrieval method described in the next subsection. The minimization of average variance corresponds to pushing off the peaks in the histogram away from each other so that the respective tissues are more distinct to each other in their intensity values. At the same time, there should not be overcontrasting which otherwise will lead to feature loss in the image. This, according to Eq. (11), will lead to increased *avar*. The image resulting from the above operation is bias free and has enhanced contrast levels between tissues. Another problem that has been addressed in the current work is the minimization of streak artifacts (whitening) at the boundaries after the homomorphic filtering. For rectifying this problem, a mask is created using region-growing algorithm to estimate the background, which is then replaced with the mean intensity value of the region of interest pixels to minimize the background while filtering.

4.2. Automatic retrieval of the number of clusters

In conventional FCM approach with neighborhood considerations [14,16], there is no provision for automatic assessment of the number of cluster centers. The method proposed by Juan et al. [28] assesses the position of the cluster centers by using weighted histogram, but this method assumes fixed number of clusters in the region of operation and, hence, leaves no room for anomaly detection such as tumor or lesions. Also, the method to detect the peaks in the histogram is quite heuristic and may lead to erroneous estimation in case two peaks lie in proximity. In the current algorithm, the number of distinct intensity regions in the bias corrected and contrasted image are calculated using HLPM, explained below.

The histogram of the image is smoothed using a running average filter of order five. After this, as a primary estimation step, we identify all the i'th bins in the histogram that satisfy the following three criteria simultaneously.

Firstly, all the local maxima in the histogram are evaluated using the following equation

$$H_i > H_j \quad \forall j \in (i-\delta, i+\delta)$$

where δ is a predefined parameter which controls the sensitivity of the algorithm for peak detection. A smaller δ would ensure detection of majority of the local peaks while a larger value for the same would lead to the detection of prominently distinct peaks only. It was experimentally observed that the best result is obtained for $\delta = 7$. However, it is to be noted that the detected peaks may not be regarded as the correct estimation of cluster centers as they may not be prominent from the global perspective. To address this issue, the following two steps are implemented.

$$H_i > \frac{\sum_{k=k_0}^{L} H_k}{2L}. \tag{13}$$

Here, L is the number of bins in the histogram. Note that a certain portion in the beginning of the histogram is constituted by the background of the MRI. Since this region accounts for a major part of the image and is observed to be restricted in a narrow intensity band near zero intensity level, the peak in the first few bins histogram is abnormally high. In order to eliminate the effect of background of the image, consideration of the bins may be begun anywhere from k_0=6 to k_0=13. In this article, the middle value, i.e., k_0=9 has been taken. Otherwise, this will lead to abnormally large values of $\left(\frac{\sum_{k=k_0}^{L} H_k}{2L}\right)$ due to its large share in the image. This criterion serves as a check so that only those points are taken as peaks which have a certain minimum value given by the above equation.

$$\sum_{k=i-i_0}^{i} \text{grad}\ (H_k) > 0 \quad \text{and} \quad \sum_{k=i}^{i+i_o} \text{grad}\ (H_k) < 0 \tag{14}$$

where i_0 is a predefined parameter and "grad" refers to gradient function. This condition eliminates those points which qualify the first two conditions due to irregular peakings in the histogram and not due to their being a distinct region of intensity.

The above process gives "primary" cluster centers. Some of these may be extraneous due to unsatisfactory peaking or close proximity of the peaks due to varied modality of the MRIs. This problem is resolved by employing an adaptive window over primary peaks. The algorithm merges two peaks, $p1$ and $p2$, and allocates as the new cluster center the

one which is higher, if the following two criteria are satisfied simultaneously

$$2H_L > \text{mean}\left(H_{p1}, H_{p2}\right). \tag{15}$$

Here, H_L is the minima between these two peaks. This introduces an adaptive vertical window of height equal to half the mean value of the two adjacent peaks [mean (H_{p1}, H_{p2})]. The two peaks are not distinct if the minima between them lies outside this window.
and,

$$|p_1 - p_2| < w_1 \text{ or } |p_1 - p_2| < w_2 \tag{16}$$

where, p_1 and p_2 are the two peaks being considered for merging, and w_p refers to an adaptive horizontal window for a peak, p, defined as

$$w_p = \left|\gamma\left(\frac{H_{p,avg}}{H_p}\right)^{\frac{1}{2}}\right|. \tag{17}$$

Here, $|x|$ represents the absolute value of any number x, and γ is a parameter used to bring the window size in the order of the range of the number of histogram levels. Histograms of a wide variety of MRIs were taken and impressive results were obtained for $\gamma=50$. $H_{p,\text{avg}}$ is the average for a peak given by

$$H_{p,\text{avg}} = \frac{\sum_{k=p-\beta}^{p+\beta} H_k}{2\beta+1}. \tag{18}$$

β defines the range of the histogram levels over which a lobe containing a peak is covered. The optimum value for β has been experimentally found to be 10. The criterion tests the proximity of the adjacent peaks being considered for merging.

The number of points (peaks) left represents the number and positions of the intensity levels recognized as initial cluster centers.

The histograms of the MRIs have been taken on 256 levels for all modalities of image formats. It is worth mentioning that the values of all the above parameters depicted amenable performance over MR scans obtained from various sources, i.e., simulated data, scans from real MRI machines, and data procured from Harvard University [(Internet Brain Segmentation Repository (IBSR)] Web site. Detailed analysis of the results has been conducted in Section 5. Evidently, the parameteric values obtained above are generic to a considerable extent.

4.3. Postprocessing using NMAC

After the application of MFCM to the unbiased and contrast-enhanced image, we obtain an interim segmented image. In the process of clustering according to the final membership function U found by MFCM, a number of pixels are encountered where the difference in their membership grades for two clusters is too low. Regions in the proximity of the boundaries have been found to be attributed with this characteristic. Pixels in such regions are marked with fairly close intensity levels and constitute a set of "ambiguous pixels." These pixels form smudged boundaries between tissue classes. In normal FCM or MFCM, such pixels are classified into that cluster for which their membership grade is maximum. However, this may lead to misclassification as the extent of belongingness to a particular class is uncertain. This poses a problem in accurately determining the area of the brain tissues and anomalies like tumor and lesions in a brain MR scan. To cater a solution for this issue, we present a method based on neighborhood effect.

We define ambiguous pixels as those in which the difference between the maximum and any other value of its membership grade is less than 0.15. The segmentation result for a tumour as shown in the box in Fig. 1A has been enlarged and shown in Fig. 1B. In this, the ambiguous pixels are shown in green color. Experimental observations for such cases show that the pixels constituting the periphery of these smudged boundaries are less ambiguous than the inner ones. Since the identification of ambiguities is dependent upon the spatially neighboring pixels, the outer pixels should be corrected first followed by the inner ones. This is because the outer pixels have greater probability of having more number

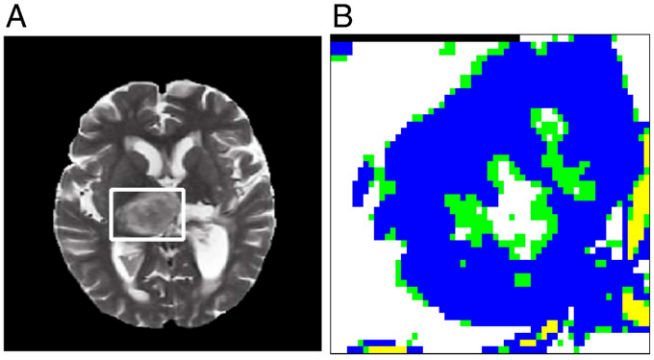

Fig. 1. (A) Real brain MRI. (B) Segmented result showing ambiguous pixels in green color for the region inside the box.

of correctly classified pixels as their neighbors as compared to the inner pixels. Taking cue from this hypothesis, the set of ambiguous pixels, A, is divided into three subsets according to the extent of ambiguity, which are given by

$$\begin{aligned} A_1 &= \{x_i | x_i \in A \ \& \ |\mu_{i1} - \mu_{i2}| < 0.05\}, \\ A_2 &= \{x_i | x_i \in A \ \& \ 0.05 \le |\mu_{i1} - \mu_{i2}| < 0.1\}, \\ A_3 &= \{x_i | x_i \in A \ \& \ 0.1 \le |\mu_{i1} - \mu_{i2}| < 0.15\} \end{aligned} \tag{19}$$

Such that

$$A = A_1 \cup A_2 \cup A_3 \tag{20}$$

where, x_i represents the i'th pixel in the image and μ_{i1} is max $\{\mu_{ij}\}$ and μ_{i2} is max $\{\mu_{ij} \backslash \mu_i 1\}$ $\forall j \in \{1,\ldots,c\}$ and c is the number of cluster centers.

We define C as the set of correctly classified pixels given by

$$C = \{x_i | x_i \notin A\}. \tag{21}$$

The sets A_3, A_2 and A_1 represent the increasing orders of ambiguity.

We first consider N as the set of nearest neighbors of the i'th pixel where $x_i \in A_3$. We define N_c as the set of neighboring pixels of i'th pixel which are distinctly classified as is given by

$$N_c = N \cap C. \tag{22}$$

Consider θ_{ik} such that

$$\theta_{ik} = \begin{cases} 1 \text{ if } \mu_{ik} = \mu_{i1} \\ 0 \text{ otherwise} \end{cases} \tag{23}$$

Now, the i'th pixel belongs to the kth cluster if

$$\sum_{x_i \in N_c} \theta_{ik} = \max\left\{ \sum_{x_i \in N_c} \theta_{ij} \right\} \ \forall j \in \{1, \ldots, c\} \tag{24}$$

If the above equation becomes valid for some other cluster, l, also, then the i'th pixel belongs to the kth cluster if

$$\sum_{x_i \in N_c} \mu_{ik} > \sum_{x_i \in N_c} \mu_{il}. \tag{25}$$

otherwise it belongs to l.

The above procedure is repeated for all the points of A_3 after which we proceed onto points of A_2 and then finally to A_1. This process significantly improves segmentation results, especially in cases of noisy scans.

The overall algorithm can be schematically represented by the block diagram shown in Fig. 2.

5. Experiments and results

In this section, we evaluate the performance of the proposed algorithm. We first present the utility of the preprocessing steps of homomorphic filtering, HTRCE, estimation of the number of cluster centers along with their initial positions and NMAC. This is followed by qualitative as well as quantitative discussions of the results. Lastly, we compare the results of our algorithm against conventional MFCM along with Yale University's BioImage Suite [29] which is built around the package FMRIB's Automated Segmentation Tool and Brain Extraction Tool [present in FMRIB's Software Library (FSL)] [17] developed by Oxford University. The FSL software employs EM algorithm coupled with hidden MRF model for segmentation problems [30] and has achieved wide acceptance. The testing is done both on real brain scans obtained from Pancham MRI Center, Bareilly, India, as well as on the simulated database available from BrainWeb simulator repository [18]. MINC files and phantoms for normal anatomical brain have been taken from BrainWeb. The modalities include scans with noise 0% to 9% of both 0% and 40% inhomogeneity. File format conversions from MINC to DICOM have been done using Microview-3D Volume Viewer and Analysis Software [31]. BrainSuite2 [32] has been used for skull striping of the various MRIs used. This is done to prevent erroneous results which may occur because of the inclusion of skull and other brain tissues of same intensity level, e.g., fat tissues, in the same cluster.

Parameter values used in the algorithm have been obtained through rigorous improvisation and are tested over a variety of images obtained from different MR imaging machines and also on simulated images. These values have been kept fixed for all the test images taken and satisfactory results have been obtained with these. This shows that although there are a range of different user-defined parameters in the current algorithm, they need to be estimated only once.

The segmentation was executed using both, four and eight nearest neighbors. The improvement in results with eight nearest neighbors was found to be insignificant but was accompanied with almost twice the computational time. Hence, for all segmentation experiments, four nearest neighbors have been considered.

Performance evaluation of the algorithm commences with the depiction of the utility of pre-processing step,

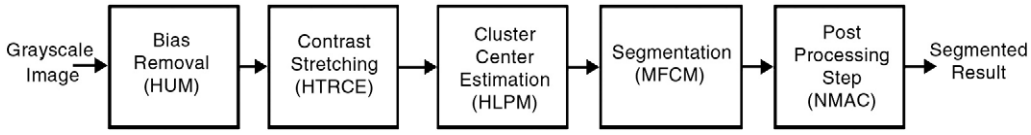

Fig. 2. Block diagram of the proposed algorithm.

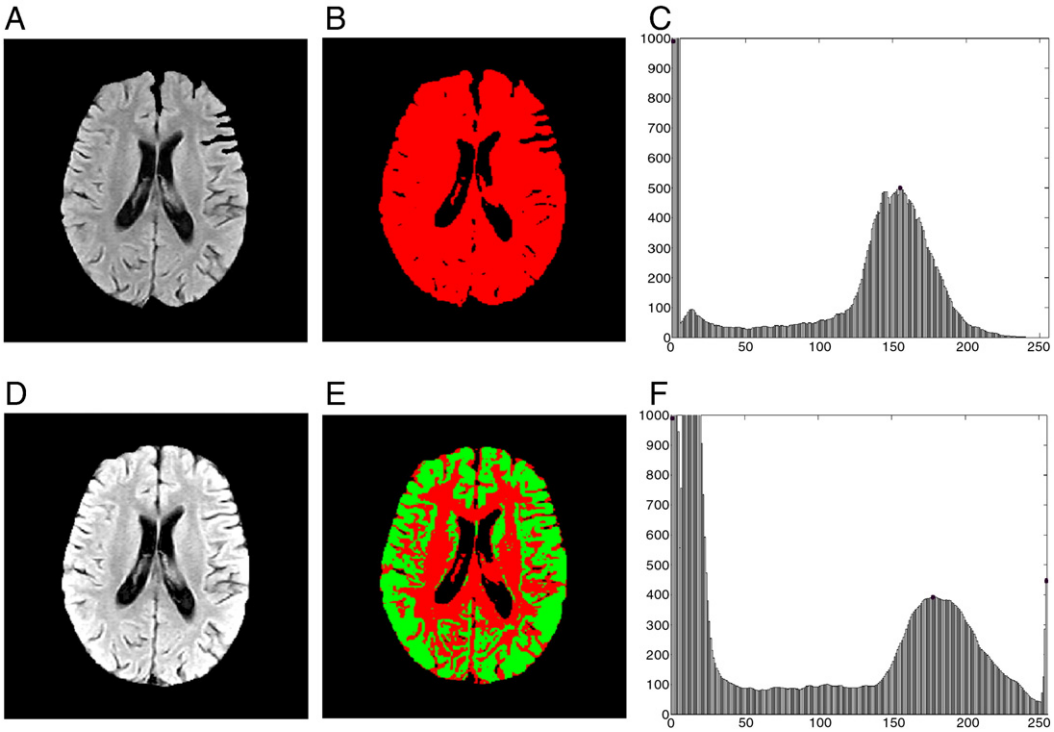

Fig. 3. (A) Original image. (B) Image segmented by modified FCM without the pre-processing step. (C) Histogram of the gray tone image without the pre-processing step along with the points identified as cluster centers. (D) Image obtained after the pre-processing step. (E) Image segmentation with the pre-processing step. (F) Histogram of the gray tone image with the preprocessing step along with the points identified as cluster centers.

i.e., homomorphic filtering technique followed by HTRCE. Here, we present how contrast enhancement makes tissue classes more distinctly identifiable. They are then correctly located by our method of automatic cluster retrieval. For this, we take a real T2-weighted brain scan with TR=6860 and TE=78. As is evident from Fig. 3A, it is quite difficult to distinguish between GM and WM. Due to this, HLPM yields only two distinct regions in the gray level histogram of the original image as shown in Fig. 3C. However, the same image yields three cluster centers, Fig. 3F, after the preprocessing step described in Section 4. The results shown in Fig. 3B and Fig. 3E present the inability of the first method to distinguish between the GM and WM, while the same is done quite efficiently after homomorphic filtering and HTRCE. The effect of HTRCE can be observed in the form of right-shifting of the peaks, Fig. 3F, of the histogram of the original image shown in Fig. 3C.

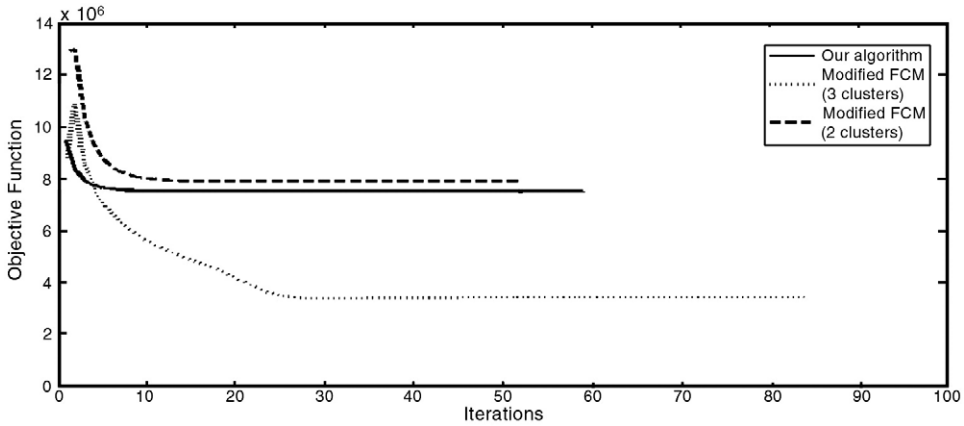

Fig. 4. Plots depicting the convergence of the objective functions for the two algorithms of modified FCM and our algorithm.

Our algorithm automatically estimates three cluster centers because of the preprocessing steps, due to which the segmentation result as shown in Fig. 3E is better than that from MFCM segmenter (Fig. 3B). The reason for identification of only two cluster centers in the unprocessed image can be attributed to its distributed histogram. Even if the number of cluster centers is manually made three in MFCM segmenter, then also the segmentation results are not comparable to that obtained from our algorithm. The result is also supported by the objective function plot for the three cases as shown in Fig. 4. It should be noted here that MFCM, in this case, takes 86 iterations, whereas our algorithm takes just 60 iterations. Since same calculations are observed in both the cases, the time duration for each iteration is same for both the cases. The bold line represents the objective function trend for our algorithm (with automatically extracted three cluster centers). The dotted and the dashed lines represent the objective functions for the MFCM segmenter with three and two randomized initial cluster centers, respectively. This set of results demonstrates the utility of predetermination of probable cluster center positions.

As an example of the efficiency of the preprocessing step, two segmentation results of tumorous real brain MR scans are shown in Fig. 5. The input images in Fig. 5A and Fig. 5C are T2-weighted MR scans with TR=4940 and TE=112. Image in Fig. 5G is a simulated normal brain image obtained from BrainWeb and Fig. 5G shows MRI made available by Harvard University (IBSR) [33]. As can be observed in Fig. 5A, the intensity of the affected region is marginally different from the WM tissues, while the tumor in the scan in Fig. 5C has diffused boundary. Still, impressive tissue classification have been observed for both the images marked with clear boundaries. Notable segmentation is observable for the other two cases as well. Although, some nontumorous regions have been classified as tumorous tissues in Fig. 5B and 5D, the algorithm achieves it's primary goal of overting the otherwise obscure anomalies present in the MR scans, which can be easily handled by human experts and actual tumorous region can be identified.

Now, we move onto qualitative estimation of the effect of using NMAC. Fig. 6 shows how NMAC technique removes the pixel level noise from the segmented result of a section of

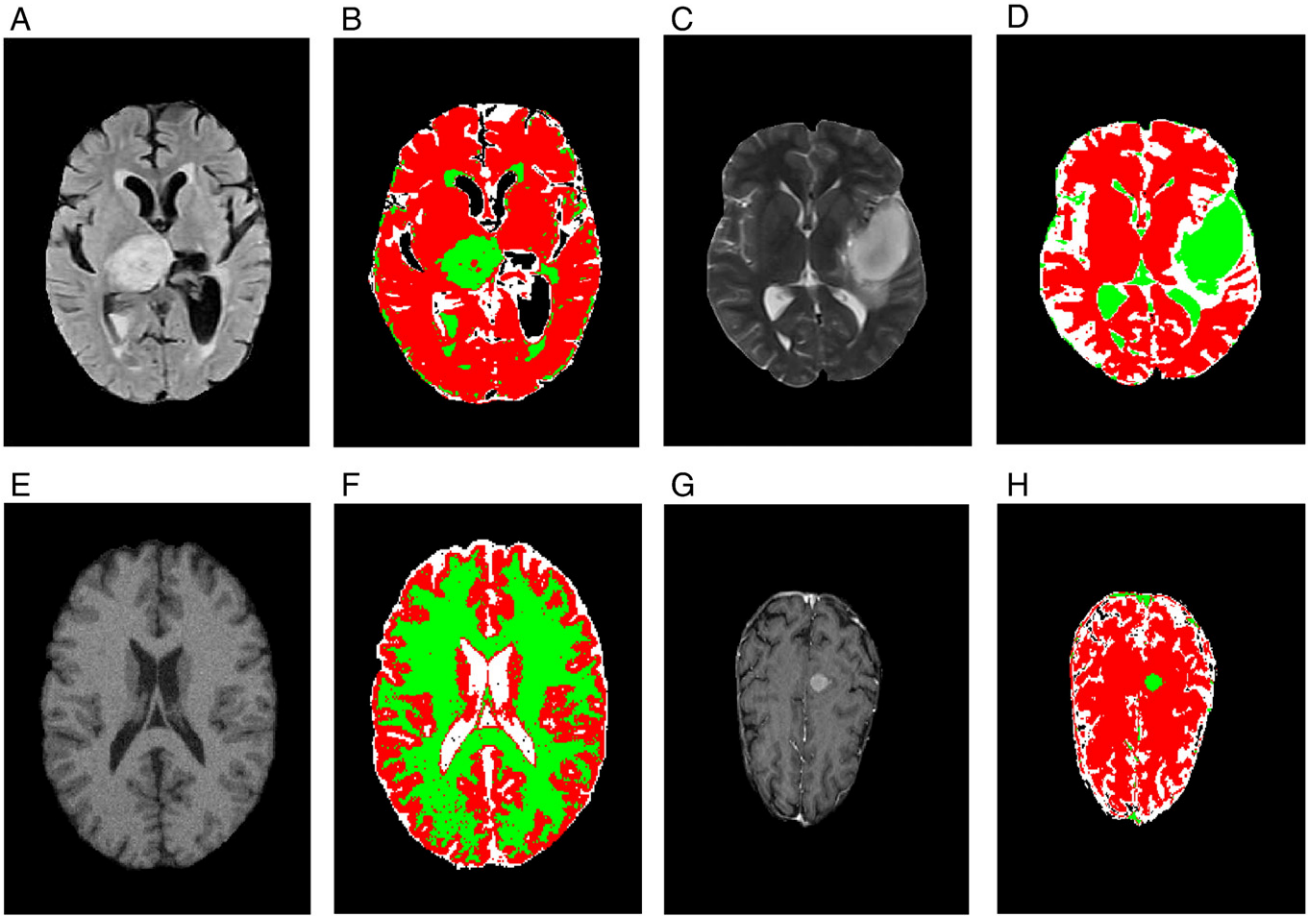

Fig. 5. (A) Real tumorous brain MRI. (B) Segmentation result for part a. (C) Real Tumorous brain MRI. (D) Segmentation result for part c. (E) Simulated brain MRI (obtained from BrainWeb). (F) Segmentation result for part e. (G) Brain MRI obtained from Harvard University Web site. (H) Segmentation result for part g.

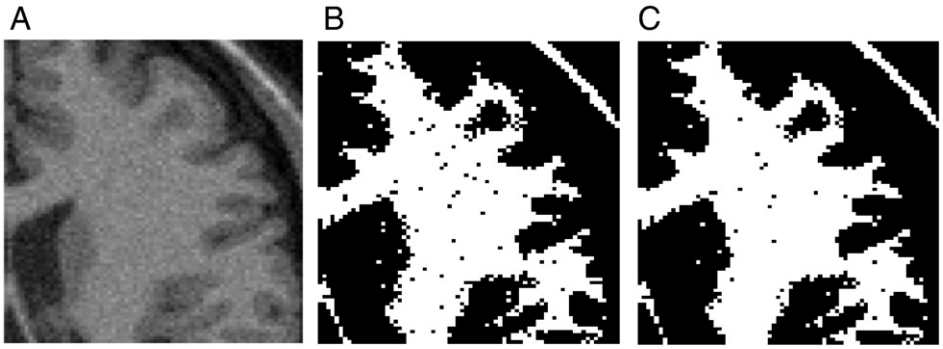

Fig. 6. (A) Synthetic image. (B) Result without NMAC. (C) Smoothed result with NMAC.

WM in a noisy simulated image. The algorithm also introduces smoothing of the boundary of the WM region.

For quantitative evaluation of the proposed algorithm, BrainWeb normal brain simulated database with noise ranging from 0–9% and inhomogeneity of 0% and 40% for each of these noise levels have been used. Performance analysis is based on three figures of merit: sensitivity (ρ), specificity (σ) [34] and similarity index (τ) [35], and comparison has been made with other established methods. Here again, phantoms available on BrainWeb repository have been taken for reference (as ground truth). It has been ensured that the algorithms under consideration work with the same number of cluster centers. For calculating these figures of merit, we first find out the true-positive (TP), true-negative (TN), false-positive (FP) and false-negative (FN) parameters for the algorithms. Pixels classified in the correct region are referred to as true; else, false. The pixels that are observed to be classified into a particular region are termed as positive, while the ones that are not are called as negatives.

Given the above four parameters, sensitivity is given as

$$\rho = \frac{\mathrm{TP}}{\mathrm{TP} + \mathrm{FN}}. \tag{26}$$

Similarly, specificity is given as

$$\sigma = \frac{\mathrm{TN}}{\mathrm{FP} + \mathrm{TN}}. \tag{27}$$

Lastly, similarity index is given by

$$\tau = \frac{2 \times \mathrm{TP}}{\mathrm{Seg} + \mathrm{Ref}} \tag{28}$$

where Seg refers to the set of pixels classified into a particular region by the current algorithm and Ref refers to the phantom-based ground truth for that region.

Though the three figures of merit are complimentary, i.e., all of them should be taken into account for segmentation result analysis, similarity index is more influential than the other two [34]. For MRI segmentation purpose, τ>0.7 has been considered as exceptionally good result [35].

Quantitative evaluation begins with the testing of NMAC. A comparison of the MRI segmentation results without and with NMAC procedure has been shown in Table 1. The rest of the algorithm has been kept identical for the two cases. This evaluation is done using different MRIs from the BrainWeb normal brain simulated database. Results for three such cases are shown in the table. The phantoms available on BrainWeb repository [18] along with these scans have been taken as the reference for comparison.

The values of similarity index, τ, as shown in Table 1 for the two sets of cases, clearly depict the improvement in results brought about by the post processing step, NMAC.

Moving on to the overall performance measurement of the proposed algorithm, as an example, for an image with 3% noise and 40% inhomogeneity, our algorithm gives τ=0.951 for GM. Result for the same as given by the widely acclaimed FSL tools for MRI segmentation developed at Oxford is .920. It can be noted that this open source software requires the manual feeding of the number of clusters.

Finally, a comparative study for the three algorithms (including the MFCM) has been presented in Table 1. In this table, a total of 12 cases have been discussed. A wide range of image modalities have been considered. This ensures that performance of the proposed algorithm is tested for most of the practically observed cases.

Table 2 shows that our algorithm outperforms MFCM in almost all the cases. Another observation is the exceptionally good performance of the BioImage (FMRIB) in terms of ρ values for WM. However, the same parameter shows quite lower values for GM. The reason for this is that the segmentation of WM by BioImage produces a result which almost fully encompasses the phantom area and hence, according to Eq. (26), the value of sensitivity comes out to be

Table 1
A comparative study of the effect of using NMAC

MR Scan modality	Without NMAC			With NMAC		
	Sensitivity (ρ)	Specificity (σ)	Similarity (τ)	Sensitivity (ρ)	Specificity (σ)	Similarity (τ)
WM						
7–20	0.9315	0.9789	0.9325	0.9341	0.9847	0.9424
7–40	0.8988	0.9824	0.9200	0.9094	0.9776	0.9301
9–20	0.8835	0.9740	0.8991	0.9078	0.9785	0.9191
GM						
7–20	0.8852	0.9663	0.8658	0.9116	0.9680	0.8839
7–40	0.8969	0.9568	0.8536	0.9121	0.9535	0.8658
9–20	0.8605	0.9494	0.8195	0.8833	0.9576	0.8477

very impressive. However, due to this "ballooning of the WM," the segmentation of GM produces constricted regions which results in much lower TP and, hence, lower ρ. Overall, our algorithm produces better results for more than 70% of the cases.

6. Conclusions and discussions

We have devised a fully automated methodology to segment MR scans of both diseased and normal brain. The algorithm shows promising results with both real and simulated MRI of both modalities, i.e., T1- and T2-weighted scans and, hence, can prove to be of significant utility in assisting human experts to segregate scads of MRI data. The algorithm begins with a preprocessing step where we implement automatic bias removal and contrast enhancement. This is followed by automated retrieval of mean intensity positions of various tissues detected. The corrected image is then passed on to an MFCM segmenter. The segmented result so obtained is further passed through NMAC which smoothes the ambiguous boundaries and also removes pixel level noise in between continuous regions of intensities.

The testing is done both on real brain scans obtained from Pancham MRI Center, Bareilly, India as well as on the simulated database available from BrainWeb. Results were found to be superior than those obtained using the established methods. The better results are also complemented with lesser computational costs due to lesser number of iterations required.

The performance of our algorithm was found to be better than that of the FSL library tool-based software in majority of the test cases taken.

Because of the fully automated nature of the algorithm with no human intervention, along with lesser number of iterations taken, the proposed algorithm is deemed to be a good candidate for fully automatic MRI analysis systems.

Acknowledgment

The authors wish to thank Dr. D. Kodesia, Dr. Vipin Peter and Pancham MRI Center, Bareilly, India, for providing real MRI data for testing.

Table 2
Showing the comparative performance chart of the Modified FCM, BioImage Suite (FMRIB) and our algorithm

MR scan modality	Modified FCM			BioImage suite (FMRIB)			Proposed algorithm		
	Sensitivity (ρ)	Specificity (σ)	Similarity (τ)	Sensitivity (ρ)	Specificity (σ)	Similarity (τ)	Sensitivity (ρ)	Specificity (σ)	Similarity (τ)
WM									
3–0	0.97184	0.99255	0.97792	0.87141	0.97274	0.90210	0.93470	0.98496	0.95065
3–40	0.94462	0.98892	0.95996	0.99504	0.97006	0.96684	0.95084	0.98842	0.96273
7–0	0.94019	0.96742	0.93678	0.99230	0.94928	0.94282	0.94673	0.97598	0.94853
7–40	0.89884	0.97324	0.92000	0.99494	0.96833	0.95677	0.90939	0.97764	0.93009
9–0	0.87685	0.95751	0.83804	0.98522	0.96809	0.90788	0.89810	0.96446	0.91161
9–40	0.86340	0.95953	0.88736	0.98544	0.94487	0.93500	0.87500	0.96976	0.90360
GM									
3–0	0.88889	0.97905	0.90733	0.866138	0.93987	0.83336	0.94745	0.97737	0.93267
3–40	0.95582	0.96095	0.91249	0.89461	0.98704	0.92042	0.91338	0.96290	0.95112
7–0	0.88610	0.95416	0.86745	0.84309	0.97550	0.86958	0.91634	0.95660	0.88729
7–40	0.89755	0.93743	0.85120	0.89754	0.97364	0.89808	0.91208	0.95355	0.86576
9–0	0.85161	0.92384	0.80932	0.73638	0.96860	0.79666	0.87685	0.93524	0.83804
9–40	0.85249	0.91890	0.80382	0.83370	0.96848	0.85285	0.88390	0.92641	0.83068

References

[1] Schmidt R. Comparison of magnetic resonance imaging in Alzheimer's disease, vascular dementia and normal aging. Eur Neurol 1992; 32:164–9.

[2] Ho B-C. MRI brain volume abnormalities in young, nonpsychotic relatives of schizophrenia probands are associated with subsequent prodromal symptoms. Schizophr Res 2007;1996:1–13.

[3] Clarke L, Velthizen R, Camacho M, Heine J, Vaidyanathan M, Hall L, et al. MRI segmentation: methods and applications. Magn Reson Imaging 1995;13:343–68.

[4] Yanga M-S, Linb KC-R, Liuc H-C, Lirngd J-F. Magnetic resonance imaging segmentation techniques using batch-type learning vector quantization algorithms. Magn Reson Imaging 2007;25:265–77.

[5] Clarke LP, Velthuizen RP, Phuphanich S, Schellenberg JD, Arrington JA, Silbiger M. MRI: Stability of three supervised segmentation techniques. Magn Reson Imaging 1995;11:95–106.

[6] Glass JO, Ji Q, Glas LS, Reddick WE. Prediction of total cerebral tissue volumes in normal appearing brain from sub-sampled segmentation volumes. Magn Reson Imaging 2003;21:977–82.

[7] Wells III WM, Grimson WEL, Kikinis R, Jolesz FA. Adaptive segmentation of MRI data. IEEE Trans Med Imaging 1996;15(4): 429–42.

[8] Leemput KV, Maes F, Vandermeulen D, Suetens P. Automated model-based bias field correction of MR images of the brain. IEEE Trans Med Imaging 1999;18(10):885–96.

[9] Zhou J, Chan K, Chong V, Krishnan S. Extraction of brain tumor from MR images using one-class support vector machine. Proc. IEEE Engineering in Medicine and Biology 27th Annual Conference, Shanghai, China; 2005. p. 6411–4. ahmed fuzzy.

[10] Reddick WE, Glass JO, Cook EN, Elkin TD, Deaton RJ. Automated segmentation and classification of multispectral magnetic resonance images of brain using artificial neural networks. IEEE Trans Med Imaging 1997;16(6):911–8.

[11] Mehta SB, Chaudhury S, Bhattacharyya A, Jena A. Handcrafted fuzzy rules for tissue classification. Magn Reson Imaging 2008;26:815–23.

[12] Suckling J, Sigmundsson T, Greenwood K, Bullmore ET. A modified fuzzy next term clustering algorithm for operator independent brain tissue classification of dual echo MR images. Magn Reson Imaging 1999;17:1065–76.

[13] Yanga M-S, Hua Y-J, Linb KC-R, Linc CC-L. Segmentation techniques for tissue differentiation in MRI of ophthalmology using fuzzy clustering algorithms. Magn Reson Imaging 2002;20:173–9.

[14] Ahmed MN, Yamany SM, Mohamed N, Farag A, Moriarty T. A modified fuzzy *c*-means algorithm for bias field estimation and segmentation of MRI data. IEEE Trans Med Imaging 2002;21(3): 193–9.

[15] Ardizzone E, Pirrone R, Gambino O. Exponential entropy driven hum on knee MR images. Proc. IEEE Engineering in Medicine and Biology 27th Annual Conference, Shanghai, China; 2005. p. 1769–72.

[16] Yong LPY, Chongxun Z. A novel fuzzy c-means clustering algorithm for image thresholding. Meas Sci Rev 2004;4:11–9.

[17] Smith SM, Jenkinson M, Woolrich MW, Beckmann CF, Behrens TE, Heidi Johansen-Berg PRB, et al. Advances in functional and structural MR image analysis and implementation as FSL. NeuroImage 2004;23: 208–19. URL www.fmrib.ox.ac.uk/fsl.

[18] Kwan RK -S, Evans AC, Pike GB. MRI simulation-based evaluation of image-processing and classification methods. IEEE Trans Med Imaging 1999;18(11):1085–97. URL http://www.bic.mni.mcgill.ca/brainweb.

[19] Pal NR, Bezdek JC. On cluster validity for the fuzzy *c*-means model. IEEE Trans Fuzzy Syst 1995;3:370–9.

[20] Arnold JB, Liow J -S, Schaper KA, Stern JJ, Sled JG, Shattuck DW, et al. Qualitative and quantitative evaluation of six algorithms for correcting intensity nonuniformity effects. Neuroimage 2001;13: 931–43.

[21] Tincher M, Meyer CR, Gupta R, Williams DM. Polynomial modeling and reduction of RF body coil spatial inhomogeneity in MRI. IEEE Trans Med Imaging 1999;12(2):361–5.

[22] Guillemaud R, Brady M. Estimating the bias field of MR images. IEEE Trans Med Imaging 1997;16(3):238–51.

[23] Rouainia M, Medjram MS, Doghmane N. Brain MRI segmentation and lesions detection by EM algorithm. Proc of World Academy of Science, Engineering and Technology, Vol. 17; 2006. p. 1307–6884.

[24] Meyer CR, Bland PH, Pipe J. Retrospective correction of intensity inhomogeneities in MRI. IEEE Trans Med Imaging 1995;14(1): 36–41.

[25] Liew AW-C, Yan H. An adaptive spatial fuzzy clustering algorithm for 3-D MR image segmentation. IEEE Trans Med Imaging 2003;22(9): 1063–75.

[26] B. Mackiewich, Intracranial boundary detection and radio frequency correction in magnetic resonance images, Master's thesis, Simon Fraser University, Canada (1995).

[27] Pratt WK. Digital Image Processing. Los Altos (CA): John Wiley & Sons, Inc; 2001. Ch. 10.

[28] He SJ, Weng X, Yang Y, Yan W. MRI brain images segmentation. Circuits and Systems, 2000. IEEE APCCAS 2000. The 2000 IEEE Asia-Pacific Conference on, Tianjin, China; 2000. p. 113–6.

[29] Bioimage suite: An integrated medical image analysis suite. URL http://www.bioimagesuite.org/.

[30] Zhang Y, Brady M, Smith S. Segmentation of brain MR images through a hidden Markov random field model and the expectation-maximization algorithm. IEEE Trans Med Imaging 2001;20(1): 45–57.

[31] Microview - 3d volume viewer. URL microview.sourceforge.net.

[32] Brainsuite2. URL http://brainsuite.usc.edu/.

[33] Internet brain segmentation repository (IBSR). URL http://www.cma.mgh.harvard.edu/ibsr/data.html.

[34] Anbeek M, Vincken KL, van Bochove GS, van Osch MJ, van der Grond J. Probabilistic segmentation of brain tissue in MR imaging. NeuroImage 2005;27(4):795–804.

[35] Zijdenbos AP, Dawant BM, Margolin RA, Palmer AC. Morphometric analysis of white matter lesions in MR images: method and validation. IEEE Trans Med Imaging 1994;13(4):716–24.